

# LGQ: Learning Discretization Geometry for Scalable and Stable Image Tokenization

Idil Bilge Altun

ialtun@iu.edu

Indiana University Bloomington  
School of Informatics, Computing,  
and Engineering  
Bloomington, IN, USA

Mert Onur Cakiroglu

meocakir@iu.edu

Indiana University Bloomington  
School of Informatics, Computing,  
and Engineering  
Bloomington, IN, USA

Elham Buxton

esahe2@uis.edu

University of Illinois Springfield  
Computer Science  
Springfield, IL, US

Mehmet Dalkilic

dalkilic@iu.edu

Indiana University Bloomington  
School of Informatics, Computing,  
and Engineering  
Bloomington, IN, USA

Hasan Kurban\*

hkurban@hbku.edu.qa

Hamad Bin Khalifa University  
College of Science and Engineering  
Doha, Qatar

## Abstract

Discrete image tokenization is a central bottleneck for scalable visual generation: a tokenizer must be compact enough for efficient latent-space priors while preserving semantically important structures as well as making effective use of discrete capacity. Existing quantizers face a persistent trade-off: vector-quantized tokenizers learn flexible geometries, but often suffer from biased straight-through optimization, codebook under-utilization, and representation collapse that intensify as vocabularies scale. In contrast, structured scalar or implicit tokenizers achieve stable, near-complete utilization by construction, but rely on fixed discretization geometries that can allocate capacity inefficiently under heterogeneous, dataset-dependent latent statistics. We introduce *Learnable Geometric Quantization (LGQ)*, a discrete image tokenizer that *learns the discretization geometry end-to-end*. LGQ replaces hard nearest-neighbor lookup with temperature-controlled soft assignments, enabling fully differentiable training while recovering hard discrete assignments at inference. This design is principled: the assignments correspond to posterior responsibilities in an isotropic Gaussian mixture and minimize a variational, free-energy objective, while provably recovering hard nearest-neighbor quantization in the low-temperature limit. To ensure confident discretization and robust scalability, LGQ combines a token-level peakedness regularizer with a global usage regularizer that discourages imbalanced marginal code utilization, preventing collapse without imposing rigid grids. Under a controlled VQGAN-style backbone on ImageNet across different vocabulary sizes, LGQ yields stable optimization and consistently balanced utilization. LGQ improves reconstruction quality over collapse-prone VQ tokenizers and matches or exceeds strong baselines such as FSQ and SimVQ, **achieving 11.88% better rFID with 49.96% lower effective representation rate** compared to FSQ, and **6.06% rFID with 49.45% lower effective representation rate** with SimVQ, showing comparable fidelity with substantially

fewer active codebook entries. Our GitHub repository is available at: <https://github.com/KurbanIntelligenceLab/LGQ>.

## Keywords

Image Tokenization, Vector Quantization, Discrete Representation Learning, Generative Models

## ACM Reference Format:

Idil Bilge Altun, Mert Onur Cakiroglu, Elham Buxton, Mehmet Dalkilic, and Hasan Kurban. . LGQ: Learning Discretization Geometry for Scalable and Stable Image Tokenization. In *Proceedings of ACM SIGKDD Conference on Knowledge Discovery and Data Mining (KDD)*. ACM, New York, NY, USA, 11 pages.

## 1 Introduction

Large-scale multimodal generative models—encompassing images, video, audio and text—have propelled discrete representation learning from a niche technique to a central pillar of modern machine learning. Discrete tokens provide a universal currency for compressing heterogeneous signals, enabling autoregressive and diffusion priors to operate on compact codes rather than raw high-dimensional data. In particular, vector-quantized variational autoencoders (VQ-VAEs) convert continuous encoder outputs into discrete codes by replacing each latent vector with its nearest neighbour in a learned codebook [13]. This simple bottleneck produces low-entropy latent sequences that can be fed into large language models or used as conditioning variables, and has powered state-of-the-art generative systems ranging from text-to-image diffusion models to speech synthesis. However, classical VQ schemes break down when one attempts to scale vocabulary sizes and model capacities to the levels demanded by cutting-edge generative tasks. Because only selected codes receive gradient updates, unused entries remain frozen; simply enlarging the vocabulary therefore fails to increase representational power. Practitioners attempt to mitigate collapse with heuristics such as codebook reseeding, commitment losses, or reservoir sampling, but these add complexity and do not fundamentally solve the problem. A robust tokenizer for next-generation generative models must address collapse at its root [17].

\*Corresponding author

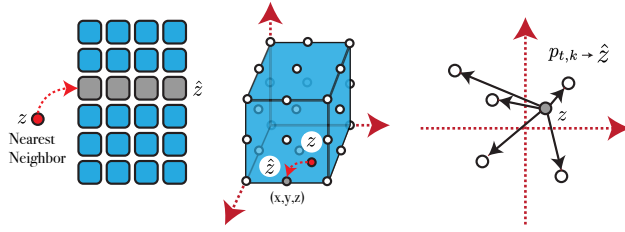


**Figure 1: Discretization geometries in latent tokenizers.** (Left:) VQ maps  $z$  to the nearest learned codeword  $\hat{z}$  (Voronoi partitions). (Middle:) FSQ quantizes each dimension with fixed axis-aligned bins (implicit lattice). (Right:) LGQ (ours) uses temperature-controlled soft assignments  $p_{t,k}$  with straight-through hard selection, learning discretization geometry end-to-end for smoother optimization and balanced utilization.

Recent attempts to mitigate collapse have revisited the optimization procedure itself. A key insight is that standard VQ performs *disjoint* codebook updates: only the nearest codeword is updated per latent token, leaving most entries inactive. Approaches such as SimVQ [17] address this by reparameterizing the codebook through a latent basis so that all codes are updated jointly. While this remedy increases utilization, it still relies on hard nearest-neighbour assignments and requires careful tuning to avoid collapse during training. When scaling to large vocabularies or highly non-linear encoders, such techniques often underperform. At the opposite extreme, *finite scalar quantization* (FSQ) dispenses with vector codebooks entirely. FSQ projects latent vectors onto a small number of scalar channels and quantizes each channel to a fixed set of values. The resulting codebook is an implicit lattice with cardinality equal to the product of channel resolutions. FSQ thereby guarantees full code utilization and eliminates the machinery of commitment losses and code resets. Unfortunately, this stability derives from rigidity: each dimension is quantised independently on a fixed grid, implicitly assuming that latent dimensions are axis-aligned and homogeneously distributed. Real-world representations are typically heterogeneous, anisotropic and dataset-dependent; fixed scalar grids often misalign with the natural data manifold and squander capacity [9].

**Bridging VQ and FSQ.** The dichotomy between the geometric flexibility of VQ and the robustness of FSQ motivates the search for a middle ground: a tokenizer that learns its discretization geometry from data while providing smooth, differentiable assignments that update all codes. Such a mechanism would allow large codebooks to be used effectively, adapt to complex latent distributions, and eliminate collapse without heavy heuristics.

**Learnable Geometric Quantization.** We propose LGQ, a unified framework that resolves the above trade-offs and elevates tokenization from an empirical hack to a principled inference problem. Figure 1 summarizes the discretization geometries induced by classical VQ, structured scalar quantization (FSQ), and our proposed LGQ, highlighting the trade-off between geometric flexibility, optimization stability, and codebook utilization. LGQ maintains a shared learnable codebook  $C = \{c_1, \dots, c_K\}$  and assigns each latent vector

$z_{e,t}$  via a temperature-controlled Gibbs distribution over Euclidean distances:

$$p_{t,k} \propto \exp(-\|z_{e,t} - c_k\|_2/\tau).$$

These soft assignments are exactly the posterior responsibilities in an isotropic Gaussian mixture model and arise as the minimizer of a variational free-energy objective (expected distance plus entropy). During training, the assignments are differentiable, allowing gradients to flow to *every* codeword and eliminating disjoint updates; during inference, a straight-through estimator converts soft assignments into discrete indices. By moving from hard nearest neighbours to Gibbs distributions, LGQ learns its discretization geometry end-to-end from data, adapting to the intrinsic structure of encoder outputs. To avoid collapse and encourage balanced usage, LGQ introduces two complementary regularizers. A token-level *peakedness* term penalises high-entropy assignments, promoting confident (near one-hot) selections without forbidding smoothness. A global usage regularizer minimizes the squared L2 norm of the empirical code usage distribution, penalising concentrated allocation and encouraging balanced utilization across codebook entries. These terms operate at different scales and jointly ensure that all codewords receive meaningful updates, thereby sustaining utilization across vocabulary sizes.

**Practical Impact and Contributions.** From a systems perspective, LGQ is a drop-in replacement for existing discrete tokenizers in autoencoder architectures. Its fully differentiable assignments obviate commitment losses and codebook reseeding and enable large vocabularies to be trained effectively. In our experiments under a VQGAN-style encoder-decoder backbone [2], LGQ achieves comparable or better reconstruction fidelity on ImageNet at lower effective representation rates and exhibits smooth optimization dynamics.

In summary, our contributions are (i) We propose Learnable Geometric Quantization (LGQ), a discrete tokenizer that learns discretization geometry via temperature-controlled Gibbs assignments, bridging VQ and FSQ. (ii) We provide theory and regularization with a variational free-energy formulation, convergence to hard quantization, Lipschitz stability, and peakedness and usage regularizers to prevent collapse. (iii) We validate empirically on ImageNet where LGQ achieves competitive rate-distortion performance with stable training and balanced utilization with increasing vocabulary size.

## 2 Background and Related Work

Discrete latent representations are a cornerstone of modern large-scale generative modeling, enabling efficient compression and tractable sequence modeling for high-dimensional data such as images, video, and audio. VQ-VAEs introduced a principled mechanism for discretization by replacing a continuous bottleneck with nearest-neighbor assignment into a learned codebook, producing discrete latent tokens suitable for autoregressive modeling [12, 13]. Hierarchical extensions such as VQ-VAE-2 further demonstrated that multi-level discrete representations can substantially improve fidelity and diversity at scale [10]. Recent work has shown that, when paired with a strong visual tokenizer such as MAGVIT-v2 (also known as LFQ), masked language models operating on discrete visual tokens can

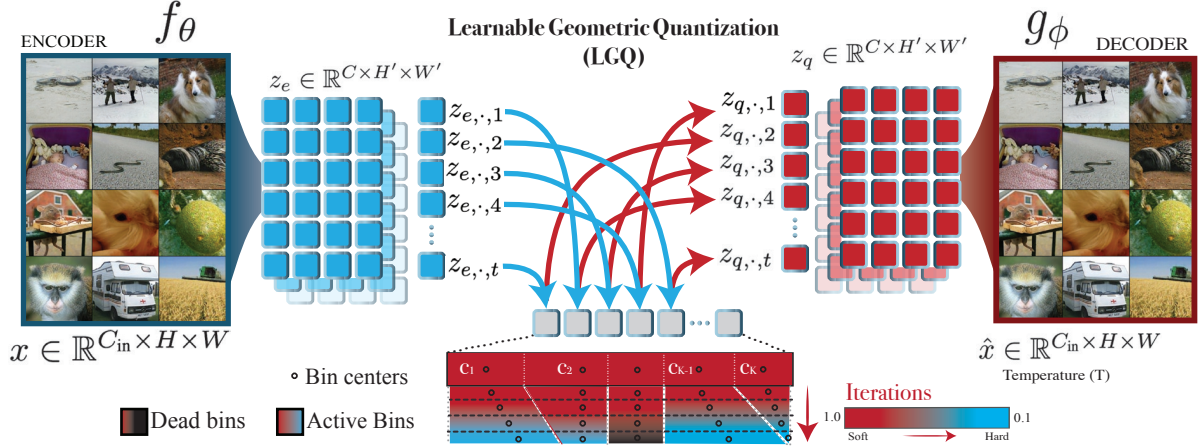


**Figure 2: LGQ-VAE pipeline.** The encoder  $f_\theta$  maps an input image  $x$  to a continuous latent representation  $z_e$ , which is discretized using *Learnable Geometric Quantization* (LGQ) before reconstruction by the decoder  $g_\phi$ . Each latent token is softly assigned to a shared learnable codebook via temperature-controlled distance-based probabilities, inducing a continuous assignment geometry over codebook entries. During training, soft assignments enable end-to-end optimization of both encoder and codebook geometry; as the temperature is annealed, assignments gradually sharpen and converge to hard quantization. The bottom panel illustrates how active codebook entries adapt to the latent distribution over training iterations, with inactive (“dead”) bins remaining unused. This soft-to-hard discretization mechanism allows LGQ to learn an efficient, data-aligned quantization structure, avoiding fixed grids and hard nearest-neighbor assignments used in standard VQ-VAEs.

outperform diffusion models in both generation quality and efficiency, highlighting the central role of tokenization in large-scale visual generative modeling [14].

## 2.1 Optimization challenges: biased gradients and representation collapse

Despite their empirical success, VQ-based tokenizers suffer from fundamental optimization challenges. A persistent challenge is the representation collapse, encompassing both token collapse (where only a small subset of codes is used) and embedding collapse (where continuous latents cluster around a few centroids). These effects become increasingly severe as vocabulary size grows, undermining scalability. Recent works propose targeted remedies, including rotation-based reparameterizations and auxiliary linear mappings, such as SimVQ, which reparameterizes the codebook via a single learnable linear transformation to jointly update the latent space and prevent code collapse [3, 17]. At the same time, scaling codebooks to extremely large vocabularies has been shown to be feasible only with explicit design choices that stabilize assignment and updates [16].

## 2.2 Structured and implicit quantization schemes

An alternative line of work seeks quantizers with more favorable scaling properties by imposing structure or using implicit vocabularies. FSQ replaces explicit vector codebooks with per-dimension discretization, simplifying optimization and guaranteeing full utilization while retaining competitive rate-distortion performance

[9]. Binary Spherical Quantization constructs an implicit, exponentially large discrete space by projecting latents onto a hypersphere and applying binary quantization, extending naturally to image and video tokenization [15]. Differentiable vector quantization methods such as DiVeQ adopt reparameterization-based estimators to improve gradient fidelity through discretization [11]. Multi-stage schemes, including residual quantization with implicit neural codebooks, progressively encode residual errors to increase expressivity for latent autoregressive generation [6, 8]. Beyond compression, quantization has been employed as an inductive bias to encourage disentanglement [4] and to study self-organizing discrete representations [7].

## 2.3 Latent geometry and downstream sequence modeling

Beyond rate-distortion trade-offs, the geometry of the latent space induced by a tokenizer plays a decisive role in downstream sequence modeling. Recent work shows that stabilizing the latent space is critical for image autoregressive models as well [18]. These findings point to three key desiderata for next-generation tokenizers: (i) scalable discrete capacity, (ii) robust optimization through or around the quantization operation, and (iii) latent geometries that are well aligned with transformer priors.

## 2.4 Motivation for Learnable Geometric Quantization

LGQ is designed to address these challenges in a unified and principled manner. Recent work has shown that fully differentiable soft assignment schemes can substantially improve optimization stability and compression efficiency but often rely on fixed similarity

structures or token aggregation rather than learning the assignment geometry itself [1]. By framing discretization as a geometry-learning problem, LGQ replaces hard nearest-neighbor assignment with temperature-controlled, distance-based soft assignments, enabling differentiable soft assignments that update all codebook entries. Peakedness and global usage regularizers jointly promote confident assignments and balanced utilization, preventing collapse even at large vocabulary sizes. Unlike classical VQ, LGQ learns its discretization geometry end-to-end from data; unlike structured schemes such as FSQ or binary quantization, it retains the flexibility to adapt to heterogeneous latent distributions. Grounded in a variational free-energy formulation with theoretical guarantees on convergence and stability, LGQ bridges the long-standing gap between flexibility and robustness in discrete representation learning and provides a tokenizer well suited for large-scale transformer-based generative modeling.

### 3 Methods

#### 3.1 Learnable Geometric Quantization

Our pipeline extends the classic VQ-VAE framework by replacing purely hard assignment training dynamics with a learnable geometric discretization mechanism based on soft-to-hard assignments. An overview of the LGQ-VAE architecture and its soft-to-hard discretization process is shown in Figure 2. Given an input image  $x \in \mathbb{R}^{C_{in} \times H \times W}$ , the encoder  $f_\theta$  first generates a continuous latent representation  $z_e \in \mathbb{R}^{C \times H' \times W'}$ , where the spatial dimensions are downsampled to  $H' = H/16$  and  $W' = W/16$ . This representation is flattened into a sequence of  $T = H'W'$  latent tokens  $z_{e,t} \in \mathbb{R}^C$ . Unlike standard VQ training, which relies on purely hard assignment during optimization, we maintain a shared learnable codebook  $C = \{c_1, \dots, c_K\}$  and compute soft assignments based on feature similarity. LGQ learns a continuous assignment geometry over the codebook through temperature-controlled soft distances, allowing the discretization structure to adapt to the latent distribution. Specifically, for each token, we calculate the Euclidean distance  $d_{t,k} = \|z_{e,t} - c_k\|_2$  to every codebook entry and derive assignment probabilities  $p_{t,k}$  using a softmax distribution with temperature  $\tau$ :

$$p_{t,k} = \frac{\exp(-d_{t,k}/\tau)}{\sum_{j=1}^K \exp(-d_{t,j}/\tau)} \quad (1)$$

The soft assignment in the equation above arises as the unique minimizer of the free-energy functional

$$\mathcal{F}(p; z) = \sum_{k=1}^K p_k \|z - c_k\|_2 + \tau \sum_{k=1}^K p_k \log p_k \quad (2)$$

which trades off expected distortion and assignment entropy. To bridge the gap between continuous optimization and discrete representation, we employ a straight-through soft-to-hard estimator. While the discrete index is selected as  $k_t^* = \arg \max_k p_{t,k}$ , the quantized token  $z_{q,t}$  preserves gradient flow by combining the hard selection with a residual correction from the soft average:

$$z_{q,t} = \sum_{k=1}^K p_{t,k} c_k + \text{sg} \left( c_{k_t^*} - \sum_{k=1}^K p_{t,k} c_k \right) \quad (3)$$

where  $\text{sg}(\cdot)$  denotes the stop-gradient operator. This yields a quantized tensor  $z_q$  that is subsequently processed by the decoder to

produce the reconstruction  $\hat{x} = g_\psi(z_q)$ . This mechanism allows the model to learn the codebook geometry directly from the data via soft assignments, avoiding fixed discretization grids and the hard nearest-neighbor quantization commonly used in standard VQ-VAEs.

#### 3.2 Model Training

We optimize a composite objective function that balances reconstruction fidelity with latent space regularization. The total training objective is defined as the sum of a reconstruction term and a latent discretization term,  $\mathcal{L} = \mathcal{L}_{\text{recon}}(x, \hat{x}) + \mathcal{L}_{\text{disc}}(z_e, z_q)$ . For reconstruction, we minimize the pixel-wise L1 distance  $\mathcal{L}_{\text{recon}}(x, \hat{x}) = \|x - \hat{x}\|_1$  between the original and decoded images. The latent discretization loss  $\mathcal{L}_{\text{disc}}$  encourages consistency between continuous and quantized latents and prevents codebook collapse. It comprises the squared error between continuous and quantized latents, along with auxiliary penalties for assignment peakedness and bin usage:

$$\mathcal{L}_{\text{disc}} = \|z_q - z_e\|_2^2 + \lambda_{\text{peak}} \mathcal{L}_{\text{peak}} + \lambda_{\text{bins}} \mathcal{L}_{\text{bins}}, \quad (4)$$

where  $z_q$  and  $z_e$  are quantized and continuous latent, respectively,  $\mathcal{L}_{\text{peak}}$  is the peakedness regularizer to encourage confident token assignments and  $\mathcal{L}_{\text{bins}}$  is a global usage regularizer to prevent codebook collapse.  $\lambda_{\text{peak}}$  and  $\lambda_{\text{bins}}$  are scalar weights that control the strength of each regularizer.

$\mathcal{L}_{\text{peak}}$  is defined as the average deviation from peaked (one-hot) assignments across all tokens:

$$\mathcal{L}_{\text{peak}} = \mathbb{E}_n [\max(0, 1 - \sum_k p_{n,k}^2)] \quad (5)$$

and  $\mathcal{L}_{\text{bins}}$  is defined as the squared L2 norm of the marginal code usage distribution:

$$\mathcal{L}_{\text{bins}} = \sum_k \bar{p}_k^2 \quad (6)$$

where  $\bar{p}_k = \frac{1}{N} \sum_n p_{n,k}$  is the empirical marginal probability of code  $k$  across all  $N$  tokens. This is minimized when code usage is uniform ( $\bar{p}_k = 1/K$  for all  $k$ ) and increases as usage becomes concentrated on fewer codes (See A.4).

#### 3.3 Convergence to Hard Quantization

The temperature parameter  $\tau$  controls the stochasticity of the assignments. When  $\tau$  is large, the assignments become diffuse; as  $\tau$  becomes small, the assignments become more deterministic. We formalize this behavior.

**Theorem 3.1** (Soft-to-hard convergence). *Suppose  $c_1, \dots, c_K$  are pairwise distinct. For fixed  $z$ , the soft assignment  $p(k | z)$  defined in (1) converges to a one-hot distribution as  $\tau \rightarrow 0$ :*

$$\lim_{\tau \rightarrow 0} p(k | z) = \mathbb{I}[k = k^*(z)] \quad (7)$$

where

$$k^*(z) = \arg \min_j \|z - c_j\|_2.$$

**PROOF.** Let  $m = \min_j \|z - c_j\|_2$  and define  $\Delta_k = \|z - c_k\|_2 - m$ . Then

$$p(k | z) = \frac{\exp(-\Delta_k/\tau)}{\sum_{j=1}^K \exp(-\Delta_j/\tau)} \quad (8)$$

If  $k^*(z)$  is the unique minimizer of  $\|z - c_k\|_2$ , then  $\Delta_{k^*(z)} = 0$  and  $\Delta_j > 0$  for  $j \neq k^*(z)$ . For  $j \neq k^*(z)$  we have  $\exp(-\Delta_j/\tau) \rightarrow 0$  as  $\tau \rightarrow 0$ . Therefore the denominator converges to 1 and the only nonvanishing term in the numerator corresponds to  $k^*(z)$ . Thus  $p(k | z) \rightarrow 0$  for  $k \neq k^*(z)$  and  $p(k^*(z) | z) \rightarrow 1$ .  $\square$

### 3.4 Optimization Stability and Gradient Regularity

LGQ training involves differentiating through the soft assignments with respect to both the encoder outputs and the codebook parameters. Under bounded latent and codebook norms, these gradients are well behaved.

**Proposition 3.2** (Lipschitz continuity). *Assume  $\|z\|_2 \leq B$  and  $\|c_k\|_2 \leq B$  for all  $z$  and  $c_k$ , and that  $z$  is such that  $\|z - c_k\|_2 > 0$  for all  $k$ . Then for any  $\tau > 0$  and any two such latents  $z_1, z_2$  we have*

$$\|p(\cdot | z_1) - p(\cdot | z_2)\|_1 \leq \frac{2K}{\tau} \|z_1 - z_2\|_2 \quad (9)$$

Additionally,  $p(k | z)$  is Lipschitz-continuous in each centroid  $c_j$ .

PROOF. Let  $d_k(z) = \|z - c_k\|_2$ . Then

$$p_k(z) = \exp(-d_k/\tau)/Z(z) \quad (10)$$

with

$$Z(z) = \sum_j \exp(-d_j/\tau). \quad (11)$$

For  $d_k > 0$ ,  $\nabla_z d_k = (z - c_k)/d_k$ .

$$\nabla_z \exp(-d_k/\tau) = \exp(-d_k/\tau) \cdot (-1/\tau)(z - c_k)/d_k \quad (12)$$

$$\Rightarrow \nabla_z Z = \sum_j \exp(-d_j/\tau) \cdot (-1/\tau)(z - c_j)/d_j \quad (13)$$

$$\Rightarrow \nabla_z p_k = \frac{p_k}{\tau} \left( -\frac{z - c_k}{d_k} + \sum_j p_j \frac{z - c_j}{d_j} \right). \quad (14)$$

For each  $j$  with  $d_j > 0$ ,  $\|(z - c_j)/d_j\|_2 = 1$ .

$$\Rightarrow \|\nabla_z p_k\|_2 \leq (p_k/\tau)(1 + \sum_j p_j) = 2p_k/\tau \leq 2/\tau. \quad (15)$$

By the mean value theorem,

$$|p_k(z_1) - p_k(z_2)| \leq (2/\tau) \|z_1 - z_2\|_2 \quad (16)$$

Summing over  $k$  yields

$$\|p(\cdot | z_1) - p(\cdot | z_2)\|_1 \leq (2K/\tau) \|z_1 - z_2\|_2 \quad (17)$$

A similar argument gives Lipschitz continuity in each  $c_j$ .  $\square$

To propagate gradients through non-differentiable argmax operations, LGQ uses the straight-through estimator (STE): in the forward pass one applies  $\arg \max_k p_k(z)$  to obtain a discrete index, while in the backward pass one substitutes the derivative of  $p_k(z)$ . This estimator introduces a bias because the gradient of a one-hot vector differs from that of  $p$ . However, the bias vanishes as the

assignments become peaked during annealing. Moreover, the STE reduces gradient variance and yields stable training. For a detailed analysis we refer to [5]. Unless otherwise stated, we set the weights  $\lambda_{\text{peak}} = \lambda_{\text{bins}} = 0.005$ . Finally, to stabilize the learning dynamic, the softmax temperature  $\tau$  is annealed linearly from  $\tau_{\text{start}} = 1.0$  to  $\tau_{\text{end}} = 0.1$  over the total training epochs  $E$ :

$$\tau(e) = \tau_{\text{start}} + (\tau_{\text{end}} - \tau_{\text{start}}) \left( \frac{e-1}{E-1} \right) \quad (18)$$

## 4 Results

### 4.1 Experimental Setup

We adopt a VQGAN-style encoder-decoder backbone in all experiments to ensure a controlled and fair comparison with discretization-based approaches. The architectural components of the encoder and decoder, the latent dimensionality, and the spatial downsampling factor are kept fixed across all settings; only the discretization mechanism is varied. The encoder downsample the input image by a fixed compression factor of 16, producing a latent representation of spatial resolution  $H' = H/16$  and  $W' = W/16$  with  $C = 64$  latent channels. This configuration matches the tokenizer setup commonly used in VQGAN based pipelines and is kept constant throughout all experiments. All experiments are conducted on the ImageNet dataset resized to  $128 \times 128$ , focusing exclusively on discretization behavior and reconstruction quality. Following the LGQ formulation, the spatial dimensions of the latent representation are flattened, yielding  $T = H'W'$  latent tokens, each represented as a vector in  $\mathbb{R}^C$ . Discretization is performed using a *single shared learnable vector codebook* of size  $K = 16,384$ , with temperature-controlled soft assignments and a straight-through estimator. Evaluation focuses on reconstruction quality and discretization dynamics. We report reconstruction FID (rFID), reconstruction loss measured by mean squared error, PSNR, LPIPS and SSIM. All metrics are computed using reconstructions obtained from the discrete latent representations. For codebook utilization, we report two metrics: *active codes* (number of codebook entries used at least once) and *effective codebook size*  $K_{\text{eff}}$ , defined as the perplexity of the empirical code usage distribution

### 4.2 Reconstruction Quality and Codebook Utilization

LGQ achieves strong reconstruction quality while substantially improving over standard vector quantization, as shown in Table 1. In particular, LGQ attains the lowest reconstruction distortion in terms of rFID (110.64), outperforming all baselines, including FSQ (125.56), VQ (121.26), LFQ (118.08), and SIM-VQ (117.77). LGQ also achieves the best SSIM (0.6335) and LPIPS (0.4864), indicating improved structural fidelity and perceptual quality.

While FSQ and SIM-VQ achieve slightly lower reconstruction loss and strong PSNR, these gains are accompanied by near-complete codebook utilization by construction. In contrast, LGQ attains comparable or superior reconstruction quality while activating substantially fewer codebook entries (8,199 vs.  $\sim 16K$ ), resulting in a much lower effective rate. This demonstrates that LGQ's performance stems from learning an efficient, data-aligned discretization

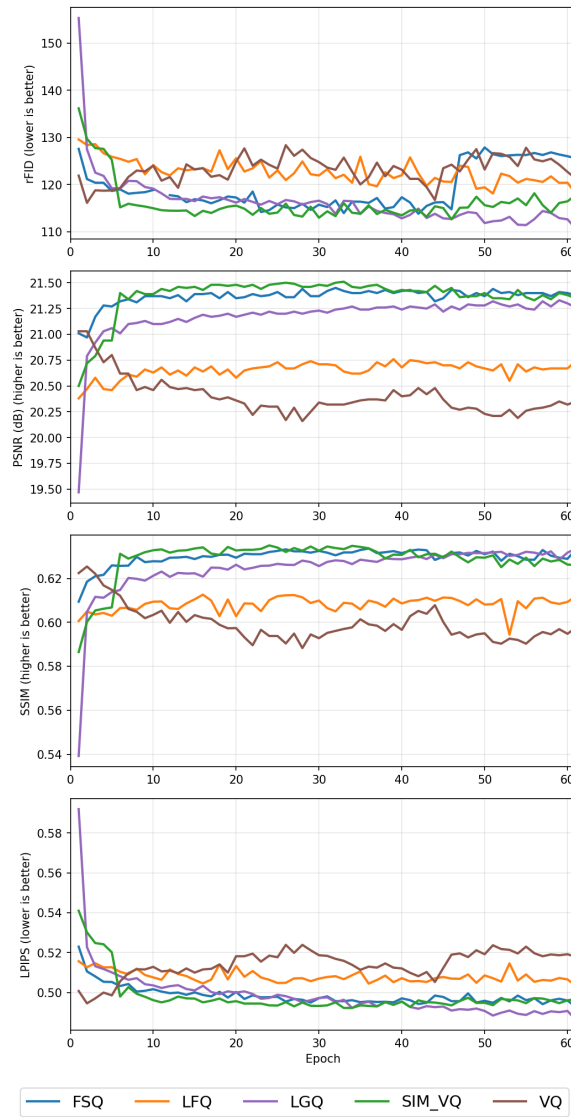


**Figure 3: Training dynamics of reconstruction quality metrics.** Per-epoch comparison of models at  $128 \times 128$  resolution over 61 training epochs. Metrics include relative Fréchet Inception Distance (rFID,  $\downarrow$ ), peak signal-to-noise ratio (PSNR,  $\uparrow$ ), structural similarity index (SSIM,  $\uparrow$ ), and learned perceptual image patch similarity (LPIPS,  $\downarrow$ ).

geometry rather than relying on codebook saturation. As further illustrated in Figure 3, LGQ exhibits smooth and stable convergence across both reconstruction and utilization metrics. Large-vocabulary scaling behavior. To assess how discretization methods behave under substantially larger vocabularies, we additionally report results at a codebook size of  $K=65,536$  in Table 1. All models are evaluated at an early training stage (epoch 9), and they provide a controlled snapshot of relative reconstruction quality and utilization trends under large codebook sizes.

**Table 1: Reconstruction quality and scaling behavior across codebook sizes. Top: main comparison at  $K=16,384$  (epoch 61). Bottom: large-vocabulary scaling at  $K=65,536$  (epoch 9). Lower rFID and reconstruction loss are better; higher PSNR, SSIM, utilization, and number of active codes indicate improved performance.**

Method	rFID $\downarrow$	PSNR $\uparrow$	SSIM $\uparrow$	Rec. Loss $\downarrow$	Util. (%)	Active
<b>Main setting: <math>K=16,384</math></b>						
FSQ	125.56	<b>21.38</b>	0.6331	0.2331	100.0	16384
LFQ	118.08	20.74	0.6118	0.2586	68.1	11165
SIM-VQ	117.77	21.35	0.6261	<b>0.2330</b>	98.9	16216
VQ	121.26	20.35	0.5975	0.2713	99.8	16358
LGQ	<b>110.64</b>	21.26	<b>0.6335</b>	0.2372	50.0	8199
<b>Large-vocabulary scaling: <math>K=65,536</math></b>						
FSQ	114.76	21.47	0.6348	<b>0.2265</b>	95.9	62860
LFQ	115.07	20.91	0.6238	0.2525	52.4	34323
SIM-VQ	125.98	20.97	0.6085	0.2418	97.8	64088
VQ	121.96	20.60	0.6075	0.2639	8.2	5391
LGQ	<b>111.08</b>	<b>21.53</b>	<b>0.6401</b>	0.2338	22.5	14716

Despite the limited number of training epochs, LGQ consistently achieves strong reconstruction quality and yielding the lowest rFID and highest SSIM while operating at substantially lower utilization compared to baselines that activate nearly the entire codebook. This indicates that LGQ can effectively allocate discrete capacity even in large-vocabulary regimes, achieving favorable reconstruction-utilization trade-offs early in training.

### 4.3 Rate–Distortion Trade-offs

While reconstruction fidelity and codebook utilization are often reported as separate metrics, their interaction is more naturally understood through a rate–distortion perspective. In this setting, distortion is measured using distributional (rFID) and perceptual (LPIPS) reconstruction metrics, while the effective representation rate reflects how much discrete capacity is actually used by the tokenizer. We first approximate the rate using empirical codebook utilization, measured by the number of active codes. Figure 6 illustrates the resulting utilization–distortion behavior across discretization methods. Methods such as FSQ and SimVQ achieve near-complete utilization by construction; however, this forced saturation does not consistently yield lower distortion. In particular, increasing utilization beyond a certain point produces diminishing returns in both rFID and LPIPS, indicating inefficient allocation of representational capacity. In contrast, LGQ achieves comparable or better distortion while operating at a significantly lower effective rate (approximately 40–55% utilization) compared to baselines that saturate the codebook. This behavior suggests that LGQ learns a discretization geometry that aligns more efficiently with the empirical latent distribution, allowing a smaller subset of codes to represent the data without sacrificing reconstruction quality, resulting in a favorable utilization–distortion trade-off.

To better understand the origin of LGQ’s favorable rate–distortion

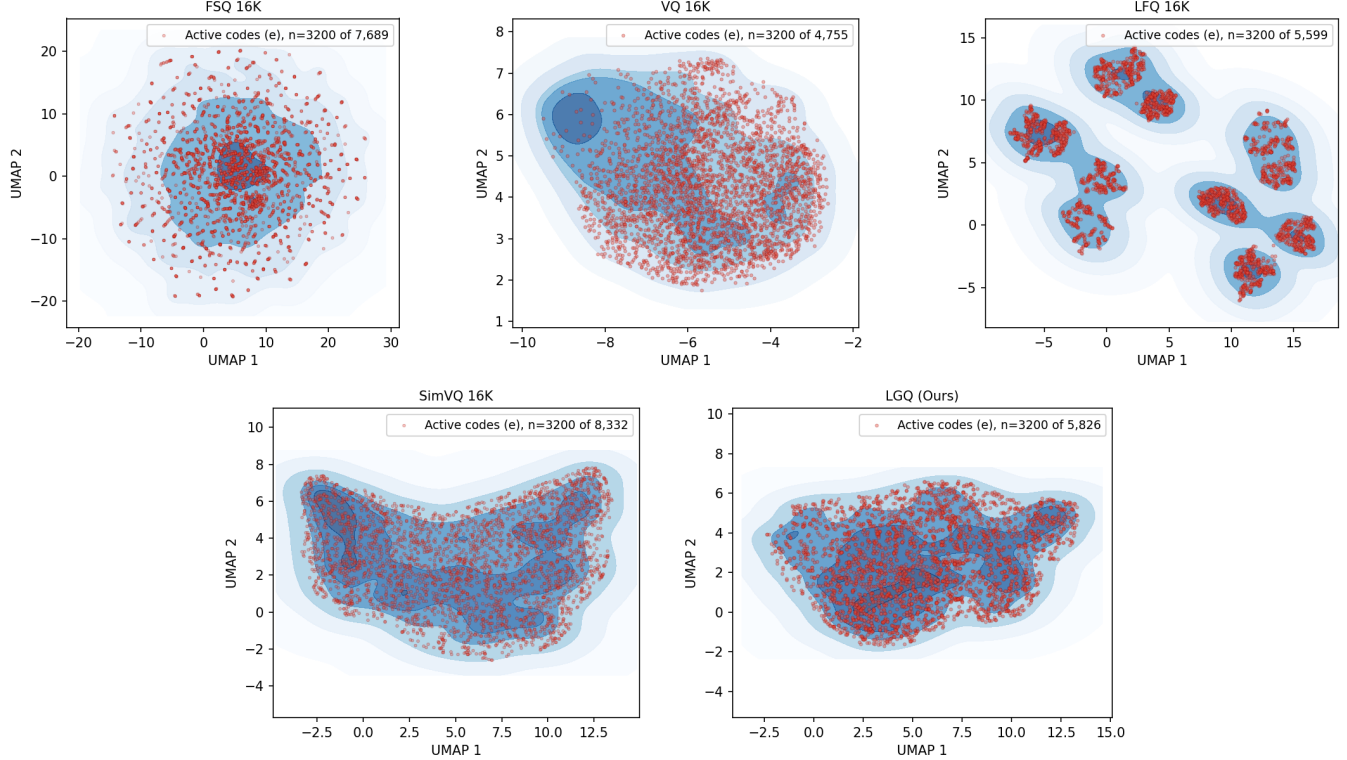


**Figure 4: Visualization of encoder outputs (blue) and active codebook entries (red) using UMAP.** Blue contours represent the density of encoder outputs, while red points denote active codebook entries. The latent distributions differ across methods as each quantizer is trained end-to-end with its own encoder; the relevant comparison is the alignment between codes (red) and latent density (blue) within each plot, not the shape of the latent space across plots. SimVQ achieves dense coverage of the latent manifold by activating nearly the entire codebook, whereas LGQ attains comparable coverage using substantially fewer active codes. This illustrates that LGQ allocates codebook capacity more selectively, supporting similar reconstruction quality at lower effective representation rates.

behavior, we relate the utilization–distortion curves in Figure 4 to the latent space visualizations in Figure 6. The UMAP projections reveal that LGQ activates a compact but well-aligned subset of codebook entries that closely follow the high-density regions of the encoder latent distribution. Despite using only approximately 50% of the available codebook, the active LGQ codes collectively span the full latent manifold, providing coverage comparable to methods such as SimVQ that activate nearly the entire codebook. This geometric alignment directly explains the improved rate–distortion trade-off observed for LGQ. Taken together, these results show that LGQ’s advantage does not arise from increased representational capacity, but from more efficient allocation of that capacity. By learning a discretization geometry that adapts to the empirical latent distribution, LGQ concentrates active codes where they are most useful, achieving better reconstruction quality while operating at a lower effective rate. This coupling between learned latent geometry and rate–distortion efficiency distinguishes LGQ from fixed or uniformly utilized discretization schemes.

#### 4.4 Center Drift Magnitude

A defining characteristic of LGQ is that discretization geometry is learned end-to-end rather than being fixed by design. To verify that codebook centers actively adapt during training, we analyze their temporal evolution across epochs. Let  $\mathbf{v}_k(t) \in \mathbb{R}^C$  denote the  $k$ -th codebook vector (center of the  $k$ -th quantization cell) at epoch  $t$ , where  $K$  is the codebook size and  $C$  is the latent dimension. We define the center drift magnitude for codebook entry  $k$  as

$$\Delta_k = \|\mathbf{v}_k(T) - \mathbf{v}_k(0)\|_2,$$

where  $T$  denotes the final training epoch. Beyond endpoint displacement, we also track the mean absolute change in codebook centers between successive epochs, which provides a finer-grained view of learning dynamics over time. As shown in Figure 5, codebook centers undergo substantial movement during the early stages of training, followed by a gradual reduction in update magnitude as training progresses. This pattern indicates an initial phase of rapid geometric reorganization, during which the codebook adapts to the empirical distribution of latent activations, followed by a stabilization phase consistent with convergence. Importantly, the observed drift is neither uniform nor random: individual codebook

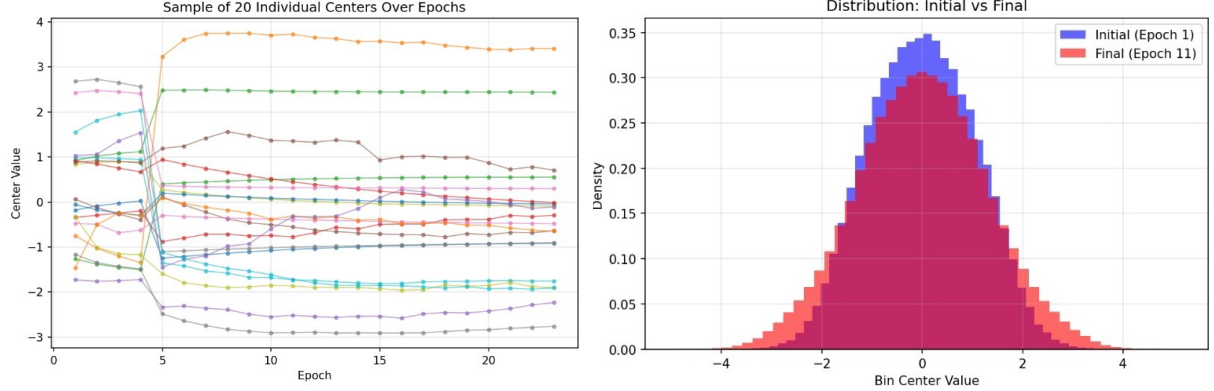


**Figure 5: Evolution of discretization bin centers during training. Right: Trajectories of a subset of individual bin centers over training epochs, highlighting structured and heterogeneous adaptation. Left: Distribution of bin center values at initialization and at the final epoch, showing a learned, non-trivial reshaping of the codebook.**

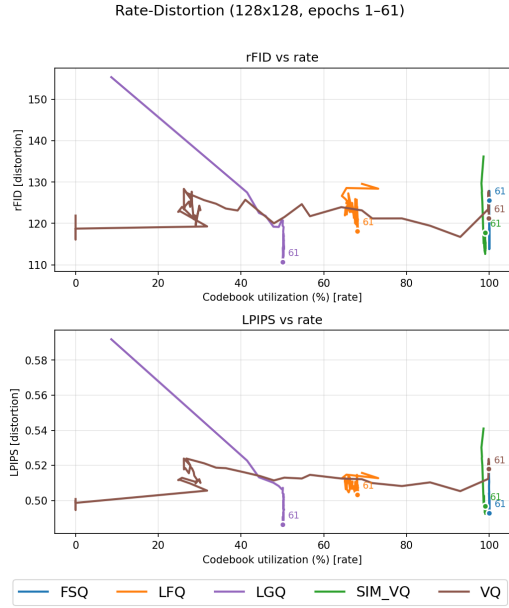


**Figure 6: Rate-distortion behavior across discretization methods.** Distortion is measured using rFID (left) and LPIPS (right), while rate is approximated by effective codebook utilization or the number of active codes.

vectors exhibit structured and heterogeneous trajectories, as evidenced by the consistent separation and relative positioning of centers over epochs. This behavior is inconsistent with trivial global shifts and instead indicates structured, data-dependent adaptation of discretization geometry. The codebook therefore functions as an adaptive quantization mechanism whose entries are optimized jointly with the encoder and decoder, rather than as a static or incidental lookup table. All reported experiments are conducted at intermediate training stages. We observe that relative trends in utilization, distortion, and geometry stabilize early, and extended

training primarily refines reconstruction metrics without altering the qualitative conclusions.

## 5 Conclusion

We introduced *Learnable Geometric Quantization (LGQ)*, a discrete image tokenizer that learns discretization geometry end-to-end via temperature-controlled soft-to-hard vector assignments. LGQ bridges the flexibility of vector quantization and the stability of structured quantizers by replacing purely hard nearest-neighbor training dynamics and fixed scalar grids with adaptive geometry learning. As a drop-in tokenizer within a controlled VQGAN-style autoencoder, LGQ yields stable optimization, confident assignments, and balanced code usage. Across the ImageNet dataset in different vocabulary sizes, LGQ consistently improves over standard VQ and matches or exceeds strong baselines such as FSQ while avoiding codebook collapse. Importantly, LGQ achieves these gains with substantially fewer *active* codebook entries, placing it at a more favorable point on the utilization–distortion frontier. These results highlight a key takeaway: utilization alone is not a sufficient measure of discretization quality—effective tokenization must allocate discrete capacity in accordance with the empirical latent distribution. By learning discretization geometry directly from data through differentiable soft assignments and regularizing for peakedness and global usage, LGQ concentrates capacity where it is most needed without resorting to brittle heuristics. More broadly, viewing quantization as *geometry learning* provides a principled foundation for designing efficient and scalable discrete representations, and motivates future extensions to latent priors and higher-dimensional tokenization (e.g., video and multimodal settings).

## 6 Limitations and Future Work

Our evaluation is restricted to ImageNet at  $128 \times 128$  resolution; validation across additional datasets, modalities (video, audio), and higher resolutions would strengthen generalizability claims. Although LGQ is designed as a general-purpose discrete tokenizer, our evaluation focuses on reconstruction and representation analysis rather than end-to-end generative modeling with a learned

prior (e.g., MaskGIT). Evaluating how learned discretization geometry impacts downstream generation quality, sampling efficiency, and training stability of token-based generators is an important direction for future work. Further experiments are needed to characterize LGQ’s scaling behavior across a wider range of codebook sizes and training durations, particularly to validate long-term convergence properties and utilization dynamics at large vocabularies. Finally, while we provide convergence and stability guarantees, formal information-theoretic rate-distortion bounds remain an open theoretical direction.

## References

[1] Hao Chen, Ze Wang, Xiang Li, Ximeng Sun, Fangyi Chen, Jiang Liu, Jindong Wang, Bhiksha Raj, Zicheng Liu, and Emad Baroumi. 2025. SoftVQ-VAE: Efficient 1-Dimensional Continuous Tokenizer. In *Proceedings of the IEEE/CVF Conference on Computer Vision and Pattern Recognition (CVPR)*. 28358–28370.

[2] Patrick Esser, Robin Rombach, and Björn Ommer. 2021. Taming Transformers for High-Resolution Image Synthesis. In *Proceedings of the IEEE/CVF Conference on Computer Vision and Pattern Recognition (CVPR)*. 12873–12883.

[3] Christopher Fifty, Ronald G. Jinkins, Dennis Duan, Aniketh Iyengar, Jerry W. Liu, Ehsan Amid, Sebastian Thrun, and Christopher Ré. 2025. Restructuring Vector Quantization with the Rotation Trick. arXiv:2410.06424 [cs.LG] <https://arxiv.org/abs/2410.06424>

[4] Kyle Hsu, William Dorrell, James Whittington, Jiajun Wu, and Chelsea Finn. 2023. Disentanglement via Latent Quantization. In *Advances in Neural Information Processing Systems*, A. Oh, T. Naumann, A. Globerson, K. Saenko, M. Hardt, and S. Levine (Eds.), Vol. 36. Curran Associates, Inc., 45463–45488. [https://proceedings.neurips.cc/paper\\_files/paper/2023/file/8e63972d4d9d81b31459d787466ce271-Paper-Conference.pdf](https://proceedings.neurips.cc/paper_files/paper/2023/file/8e63972d4d9d81b31459d787466ce271-Paper-Conference.pdf)

[5] Minyoung Huh, Brian Cheung, Pulkit Agrawal, and Phillip Isola. 2023. Straightening out the straight-through estimator: Overcoming optimization challenges in vector quantized networks. In *International Conference on Machine Learning*, PMLR, 14096–14113.

[6] Iris A. M. Huijben, Matthijs Douze, Matthew Muckley, Ruud J. G. van Sloun, and Jakob Verbeek. 2024. Residual Quantization with Implicit Neural Codebooks. arXiv:2401.14732 [cs.LG] <https://arxiv.org/abs/2401.14732>

[7] Kazuki Irie, Róbert Csordás, and Jürgen Schmidhuber. 2024. Self-organising Neural Discrete Representation Learning à la Kohonen. In *Artificial Neural Networks and Machine Learning – ICANN 2024*, Michael Wand, Kristína Malinovská, Jürgen Schmidhuber, and Igor V. Tetko (Eds.). Springer Nature Switzerland, Cham, 343–362.

[8] Doyup Lee, Chiheon Kim, Saehoon Kim, Minsu Cho, and Wook-Shin Han. 2022. Autoregressive Image Generation using Residual Quantization. arXiv:2203.01941 [cs.CV] <https://arxiv.org/abs/2203.01941>

[9] Fabian Mentzer, David Minnen, Eiríkur Agustsson, and Michael Tschannen. 2023. Finite Scalar Quantization: VQ-VAE Made Simple. arXiv:2309.15505 [cs.CV] <https://arxiv.org/abs/2309.15505>

[10] Ali Razavi, Aaron van den Oord, and Oriol Vinyals. 2019. Generating Diverse High-Fidelity Images with VQ-VAE-2. In *Advances in Neural Information Processing Systems*, H. Wallach, H. Larochelle, A. Beygelzimer, F. d’Alché-Buc, E. Fox, and R. Garnett (Eds.), Vol. 32. Curran Associates, Inc. [https://proceedings.neurips.cc/paper\\_files/paper/2019/file/5f8e2fa1718d1bbcadf1cd9c7a54fb8c-Paper.pdf](https://proceedings.neurips.cc/paper_files/paper/2019/file/5f8e2fa1718d1bbcadf1cd9c7a54fb8c-Paper.pdf)

[11] Mohammad Hassan Vali, Tom Bäckström, and Arno Solin. 2025. Di-VeQ: Differentiable Vector Quantization Using the Reparameterization Trick. arXiv:2509.26469 [cs.LG] <https://arxiv.org/abs/2509.26469>

[12] Aaron van den Oord, Oriol Vinyals, and koray kavukcuoglu. 2017. Neural Discrete Representation Learning. In *Advances in Neural Information Processing Systems*, I. Guyon, U. von Luxburg, S. Bengio, H. Wallach, R. Fergus, S. Vishwanathan, and R. Garnett (Eds.), Vol. 30. Curran Associates, Inc. [https://proceedings.neurips.cc/paper\\_files/paper/2017/file/7a98af1e63a0ac09ce2e96d03992fbc-Paper.pdf](https://proceedings.neurips.cc/paper_files/paper/2017/file/7a98af1e63a0ac09ce2e96d03992fbc-Paper.pdf)

[13] Aaron van den Oord, Oriol Vinyals, and Koray Kavukcuoglu. 2018. Neural Discrete Representation Learning. arXiv:1711.00937 [cs.LG] <https://arxiv.org/abs/1711.00937>

[14] Lijun Yu, José Lezama, Nitesh B. Gundavarapu, Luca Versari, Kihyuk Sohn, David Minnen, Yong Cheng, Vighnesh Birodkar, Agrim Gupta, Xiuye Gu, Alexander G. Hauptmann, Boqing Gong, Ming-Hsuan Yang, Irfan Essa, David A. Ross, and Lu Jiang. 2024. Language Model Beats Diffusion – Tokenizer is Key to Visual Generation. arXiv:2310.05737 [cs.CV] <https://arxiv.org/abs/2310.05737>

[15] Yue Zhao, Yuanjun Xiong, and Philipp Krähenbühl. 2024. Image and Video Tokenization with Binary Spherical Quantization. arXiv:2406.07548 [cs.CV] <https://arxiv.org/abs/2406.07548>

[16] Lei Zhu, Fangyun Wei, Yanyue Lu, and Dong Chen. 2024. Scaling the Codebook Size of VQ-GAN to 100,000 with a Utilization Rate of 99%. In *Advances in Neural Information Processing Systems*, A. Globerson, L. Mackey, D. Belgrave, A. Fan, U. Paquet, J. Tomczak, and C. Zhang (Eds.), Vol. 37. Curran Associates, Inc., 12612–12635. doi:10.52202/079017-0401

[17] Yongxin Zhu, Bocheng Li, Yifei Xin, Zhihua Xia, and Linli Xu. 2025. Addressing Representation Collapse in Vector Quantized Models with One Linear Layer. arXiv:2411.02038 [cs.LG] <https://arxiv.org/abs/2411.02038>

[18] Yongxin Zhu, Bocheng Li, Hang Zhang, Xin Li, Linli Xu, and Lidong Bing. 2024. Stabilize the Latent Space for Image Autoregressive Modeling: A Unified Perspective. arXiv:2410.12490 [cs.CV] <https://arxiv.org/abs/2410.12490>

## A Appendix

### A.1 Ablation study on the auxilary losses

Table 2 examines the influence of different temperature schedules on LGQ training stability and performance. Fast annealing yields the best overall results, achieving the lowest rFID and LPIPS while maintaining high PSNR, SSIM, and effective codebook usage. In contrast, a fixed temperature leads to inferior performance and reduced utilization, suggesting insufficient pressure toward confident discretization. Slow annealing results in catastrophic collapse, where almost all bins become inactive, severely degrading reconstruction quality. This highlights the sensitivity of LGQ to temperature dynamics and underscores the importance of sufficiently rapid annealing to encourage discrete commitment without destabilizing training.

**Table 2: Effect of temperature annealing schedule on LGQ.**

Schedule	rFID ↓	PSNR ↑	SSIM ↑	LPIPS ↓	Util. (%)	Active
Fast annealing (1.0 → 0.05)	<b>118.36</b>	<b>21.12</b>	<b>0.6257</b>	<b>0.4994</b>	57.96	9496
Fixed temperature (1.0 → 0.1)	123.50	21.01	0.6152	0.5103	46.61	7637
Slow annealing (1.0 → 0.2)	364.51	11.46	0.3339	0.8341	0.01	1

Table 4 shows that introducing either peakedness or usage regularization alone reduces codebook utilization but also degrades reconstruction quality relative to the unregularized model, indicating that each constraint in isolation enforces a suboptimal rate-distortion trade-off. In contrast, jointly applying both regularizers recovers much of the reconstruction quality while operating at a substantially lower effective rate, yielding a more favorable utilization-distortion balance.

### A.2 Matched Effective Capacity ( $K_{\text{eff}}$ )

To isolate the effect of discretization geometry from raw vocabulary size, we evaluate all tokenizers under a matched effective capacity constraint. Specifically, we restrict all methods to the same number of active codes chosen to match the natural code usage of LGQ. We set  $K_{\text{eff}}$  to the number of distinct codes used by LGQ on the validation set in one evaluation pass. For each baseline, we collect code usage counts on the same validation pass and keep the top- $K_{\text{eff}}$  most frequent codes. As shown in Table 5, LGQ achieves reconstruction distortion comparable to VQ (rFID 101.88 vs. 100.45), while outperforming FSQ and SimVQ by a substantial margin (rFID 109.01 and 120.00, respectively). At the same effective capacity, LGQ also attains the highest PSNR (22.35) among all methods, indicating improved signal fidelity at equal discrete budget. Standard VQ can marginally outperform LGQ in rFID. However, VQ requires careful tuning and collapses outside this narrow regime, whereas LGQ naturally converges to favorable operating points with lower

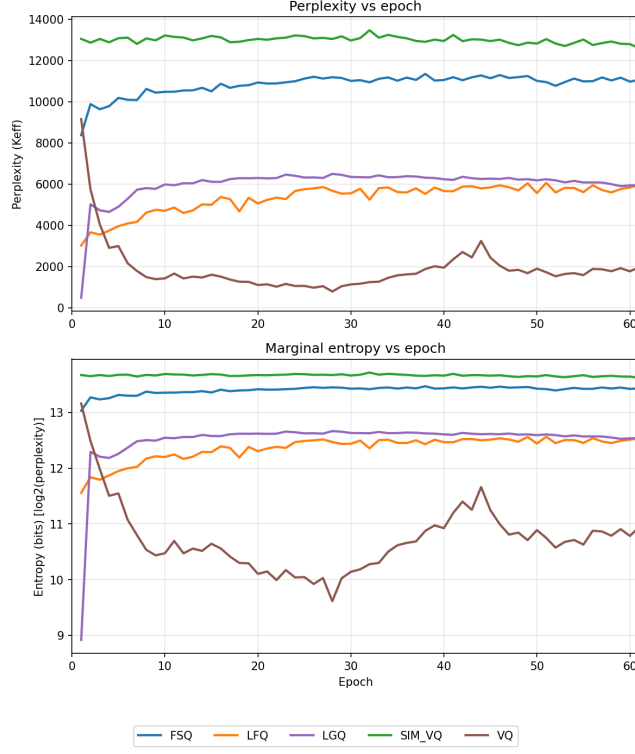


**Figure 7: Perplexity and marginal entropy dynamics over training.** Top: Effective codebook size (perplexity  $K_{\text{eff}}$ ) as a function of training epoch. Bottom: Marginal assignment entropy measured as  $\log_2(\text{perplexity})$ . FSQ and SimVQ rapidly reach near-saturated entropy, reflecting full codebook utilization by design, while VQ exhibits entropy collapse. LGQ converges to a stable intermediate entropy regime, indicating selective yet balanced use of discrete capacity that underlies its favorable rate–distortion behavior.

**Table 3: Reconstruction quality and entropy-based rate across discretization methods. Lower rFID indicates better reconstruction quality, while entropy (in bits) reflects the effective representation rate.**

Model	rFID $\downarrow$	Entropy (bits)
SIM_VQ	114.42	13.68
LGQ	115.31	12.58
FSQ	116.62	13.41
LFQ	123.48	12.39
VQ	123.47	10.56

entropy and stable utilization. LGQ’s advantage therefore lies in robustness and automatic rate selection rather than dominating VQ at fixed  $K_{\text{eff}}$ . These results suggest that LGQ’s learned discretization geometry enables competitive reconstruction quality without relying on near-saturated codebook usage, supporting the claim

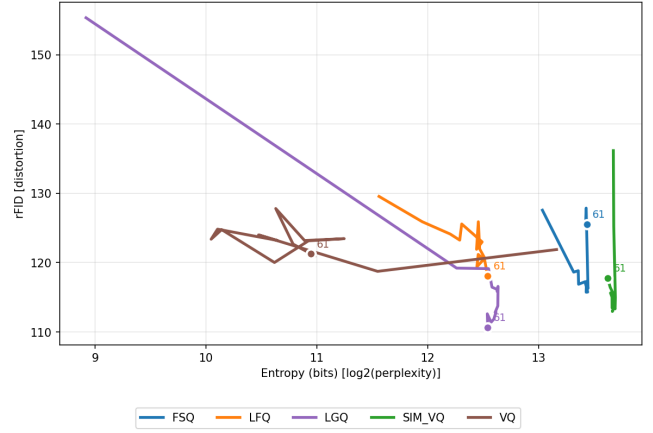


**Figure 8: Entropy-based rate–distortion analysis.** Reconstruction distortion (rFID) as a function of entropy-based rate. Each point corresponds to a different training epoch.

**Table 4: Effect of regularization on LGQ. Ablation of peakedness and usage regularization.**  
Metrics reported at epoch 2 (LPIPS computed).

Setting	rFID $\downarrow$	PSNR $\uparrow$	SSIM $\uparrow$	LPIPS $\downarrow$	Util. (%) $\uparrow$	Active
None (0, 0)	128.16	20.77	0.6044	<b>0.5240</b>	41.43	6787
Weak (0.002, 0.002)	127.31	20.84	0.6010	0.5269	36.30	5947
Bins only (0, 0.01)	127.91	20.81	0.5997	0.5283	37.37	6102
Peak only (0.01, 0)	127.66	20.87	0.5989	0.5301	39.09	6404
Strong (0.01, 0.01)	<b>126.43</b>	20.81	0.6011	0.5271	39.09	6402

that its advantages stem from more efficient allocation of discrete representational capacity rather than increased effective rate.

**Table 5: Evaluation at matched effective capacity ( $K = 8241$  active codes).**

Model	rFID $\downarrow$	PSNR $\uparrow$	SSIM $\uparrow$	Rec. Loss $\downarrow$
LGQ (Ours)	101.88	22.35	0.646	0.203
FSQ	109.01	22.13	0.639	0.212
SimVQ	120.00	21.82	0.618	0.216
VQ	100.45	22.21	0.642	0.216

### A.3 Rate Distortion via Entropy

To complement the utilization-based analysis in Section 4.3, we measure rate using marginal entropy of code usage in bits (Table 3). We first examine how different discretization methods evolve their effective rate during training. Figure 7 reports the marginal entropy (in bits) and the corresponding perplexity of code usage across training epochs. Standard VQ exhibits entropy collapse, reflecting severe codebook under-utilization. In contrast, FSQ and SimVQ operate at near-saturated entropy by construction, as their discretization schemes enforce near-uniform code usage regardless

of the latent data distribution. LGQ displays qualitatively different behavior: entropy increases during early training as the codebook reorganizes, then stabilizes at an intermediate value. This indicates that LGQ autonomously selects an effective operating rate, rather than collapsing or saturating the codebook.

We next relate this learned rate to reconstruction quality. Figure 8 plots reconstruction distortion (rFID) as a function of entropy-based rate, with each point corresponding to a different training epoch. While FSQ and SimVQ cluster at high entropy values with limited variation in distortion, LGQ traces a clear rate–distortion curve, achieving comparable or lower rFID at substantially lower entropy. This demonstrates that LGQ allocates probability mass over codes more efficiently, concentrating representational capacity in regions aligned with the empirical latent distribution.

#### A.4 Regularizer Optimality Proofs

We formally prove that the peakedness and usage regularizers introduced in Section 3.2 drive the model toward their intended behaviors. Proposition A.1 shows that minimizing  $\mathcal{L}_{\text{peak}}$  pushes each token assignment toward a peaked (one-hot) distribution, ensuring confident discretization. Proposition A.2 shows that minimizing  $\mathcal{L}_{\text{bins}}$  encourages uniform code usage across the codebook, preventing collapse.

**Proposition A.1** (Peaked assignments). *Let  $p = (p_1, \dots, p_K)$  be a categorical distribution on  $[K]$ . Then  $\sum_{k=1}^K p_k^2 \leq 1$ , with equality if and only if  $p$  is a Dirac (one-hot) distribution. Hence  $\max(0, 1 - \sum_k p_k^2) \geq 0$  with equality iff  $p$  is one-hot. Minimizing*

$$\mathcal{L}_{\text{peak}} = \mathbb{E}_n [\max(0, 1 - \sum_k p_{n,k}^2)] \quad (19)$$

*therefore, drives each assignment  $p_n$  toward a one-hot distribution.*

**PROOF.** For any probability vector  $p$ ,  $\sum_k p_k = 1$  and  $p_k \geq 0$ . By Cauchy–Schwarz,

$$1 = (\sum_k p_k \cdot 1)^2 \leq (\sum_k p_k^2)(\sum_k 1^2) = K \sum_k p_k^2 \quad (20)$$

$$\Rightarrow \sum_k p_k^2 \geq 1/K, \quad \sum_k p_k^2 \leq (\sum_k p_k)^2 = 1 \quad (21)$$

with equality iff exactly one  $p_k = 1$  and the rest zero. Thus  $\sum_k p_k^2 \leq 1$  with equality iff  $p$  is one-hot, so  $1 - \sum_k p_k^2 \geq 0$  with equality iff  $p$  is one-hot. Minimizing  $\mathcal{L}_{\text{peak}}$  thus drives each  $p_n$  toward a one-hot distribution.  $\square$

**Proposition A.2** (Balanced codebook utilization). *Let  $\bar{p} \in \mathbb{R}^K$  be a probability vector (the empirical marginal of assignments). Then*

$$\mathcal{L}_{\text{bins}} = \sum_{k=1}^K \bar{p}_k^2 \geq 1/K \quad (22)$$

*with equality if and only if  $\bar{p}$  is uniform ( $\bar{p}_k = 1/K$  for all  $k$ ). Minimizing  $\mathcal{L}_{\text{bins}}$  penalises concentrated usage and pushes  $\bar{p}$  toward uniformity.*

**PROOF.** We have  $\bar{p}_k \geq 0$  and  $\sum_k \bar{p}_k = 1$ . By Cauchy–Schwarz,

$$1 = (\sum_k \bar{p}_k \cdot 1)^2 \leq (\sum_k \bar{p}_k^2)(\sum_k 1^2) = K \sum_k \bar{p}_k^2 \quad (23)$$

so  $\mathcal{L}_{\text{bins}} = \sum_k \bar{p}_k^2 \geq 1/K$ . Equality holds iff  $(\bar{p}_1, \dots, \bar{p}_K)$  is proportional to  $(1, \dots, 1)$ , i.e.  $\bar{p}_k = 1/K$  for all  $k$ .  $\square$